© 2024. Published by The Company of Biologists Ltd | Journal of Cell Science (2024) 137, jcs261509. doi:10.1242/jcs.261509

SHORT REPORT

SPECIAL ISSUE: CELL AND TISSUE POLARITY

TIAM-1 regulates polarized protrusions during dorsal intercalation in the *Caenorhabditis elegans* embryo through both its GEF and N-terminal domains

Yuyun Zhu[1,*], Zoe Tesone[2,*], Minyi Tan[3] and Jeff Hardin[1,2,3,‡]

ABSTRACT

Mediolateral cell intercalation is a morphogenetic strategy used throughout animal development to reshape tissues. Dorsal intercalation in the *Caenorhabditis elegans* embryo involves the mediolateral intercalation of two rows of dorsal epidermal cells to create a single row that straddles the dorsal midline, and thus is a simple model to study cell intercalation. Polarized protrusive activity during dorsal intercalation requires the *C. elegans* Rac and RhoG orthologs CED-10 and MIG-2, but how these GTPases are regulated during intercalation has not been thoroughly investigated. In this study, we characterized the role of the Rac-specific guanine nucleotide exchange factor (GEF) TIAM-1 in regulating actin-based protrusive dynamics during dorsal intercalation. We found that TIAM-1 can promote formation of the main medial lamellipodial protrusion extended by intercalating cells through its canonical GEF function, whereas its N-terminal domains function to negatively regulate the generation of ectopic filiform protrusions around the periphery of intercalating cells. We also show that the guidance receptor UNC-5 inhibits these ectopic filiform protrusions in dorsal epidermal cells and that this effect is in part mediated via TIAM-1. These results expand the network of proteins that regulate basolateral protrusive activity during directed rearrangement of epithelial cells in animal embryos.

KEY WORDS: *Caenorhabditis elegans*, Cell rearrangement, Convergent extension, Morphogenesis, TIAM-1, UNC-5

INTRODUCTION

During embryonic development, cell fate specification and cellular movements work in tandem to achieve the extensive morphological changes that occur as the body plan emerges. One type of cell rearrangement, convergent extension (CE), is a ubiquitous morphogenetic movement that elongates a tissue along one axis while narrowing it along the orthogonal axis (Huebner and Wallingford, 2018; Walck-Shannon and Hardin, 2014). CE or its variants drive morphogenetic movements during gastrulation (Solnica-Krezel and Sepich, 2012), neurulation (Williams et al., 2014) and shape organogenesis in tissues such as the vertebrate lateral line and the mammalian cochlea (Driver et al., 2017; Sutherland et al., 2020). Because of its early involvement during embryonic development, failure of CE is often accompanied by severe congenital abnormalities, including craniorachischisis and spina bifida (Nikolopoulou et al., 2017).

Many studies of epithelial CE have focused on germband extension in *Drosophila*. During this process, cells shorten their anterior–posterior boundaries and extend their dorsoventral boundaries as they undergo oriented neighbor exchange (Bertet et al., 2004; Kong et al., 2017; Pilot and Lecuit, 2005). In contrast to the apical junctional dynamics that appear to drive *Drosophila* germband extension, other examples of epithelial CE rely on basolateral protrusive activity to accomplish cell rearrangement (Walck-Shannon and Hardin, 2014). Examples include the ascidian notochord, the sea urchin archenteron and the mammalian neural plate (Munro and Odell, 2002a,b; Sutherland et al., 2020; Williams et al., 2014). How basolateral protrusive activity in epithelia is controlled during tissue rearrangement is, therefore, an important question in morphogenesis.

A useful system for identifying previously unreported, conserved, functionally relevant molecular pathways that regulate basolateral protrusive activity during epithelial cell rearrangement is the dorsal epidermis of the *Caenorhabditis elegans* embryo. Dorsal epidermal cells undergo a movement known as dorsal intercalation, in which a primary, medially directed basolateral protrusion extended by each cell drives mediolateral intercalation (Walck-Shannon et al., 2015; Williams-Masson et al., 1998). The WAVE complex is constitutively required for protrusion-triggered intercalation (Patel et al., 2008; Walck-Shannon et al., 2015). Our previous work also showed that the *C. elegans* Rac family proteins CED-10 and MIG-2 promote protrusive activity in dorsal epidermal cells. In their active state, CED-10 and MIG-2 lead to the polymerization and nucleation of actin filaments and subsequent formation of lamellipodia via the WAVE and WASP complexes (Walck-Shannon et al., 2015). We also previously identified an upstream guanine nucleotide exchange factor (GEF), UNC-73 (Trio in mammals), which acts via its Rac-GEF domain to regulate Rac family proteins (Walck-Shannon et al., 2015), but other potential upstream regulators have not been thoroughly investigated.

Here, we establish a role for *C. elegans* TIAM-1, a Rac-specific GEF, in regulating protrusive activity during dorsal intercalation. In *tiam-1* mutants lacking GEF activity, dorsal epidermal cells generated less robust primary protrusions during intercalation, leading to significantly increased intercalation time. We also identified a previously unreported function for the N-terminal domains of TIAM-1 in inhibiting the formation of ectopic filiform protrusions at the cell periphery, which at least in part act independently of the GEF domain. Taken together, our data establish a role for TIAM-1 in regulating polarized protrusive

[1]Genetics PhD Program, University of Wisconsin, Madison, WI 53706, USA. [2]Cellular and Molecular Biology PhD Program, University of Wisconsin, Madison, WI 53706, USA. [3]Department of Integrative Biology, University of Wisconsin, Madison, WI 53706, USA.
*These authors contributed equally to this work

‡Author for correspondence (jdhardin@wisc.edu)

J.H., 0000-0001-7399-6580

Handling Editor: David Bryant
Received 24 July 2023; Accepted 5 February 2024

Journal of Cell Science (2024) 137, jcs261509. doi:10.1242/jcs.261509

activity during dorsal intercalation through both its GEF and N-terminal domains.

RESULTS AND DISCUSSION

tiam-1 is required for normal temporal progression of dorsal intercalation

Dorsal intercalation is driven by the mediolateral protrusive activity of dorsal epidermal cells (see Fig. 1C, wildtype). Our previous work identified the *C. elegans* Rac-GTPase orthologs CED-10 and MIG-2 as partially redundant regulators of protrusion formation via activation of the downstream Arp2/3 activators, WVE-1 (WAVE) and WSP-1 (WASP), respectively (Walck-Shannon et al., 2015). We showed previously that UNC-73 functions as a Rac-GEF in promoting protrusion formation. We also showed that, in the case of loss of function for the protein CRML-1 (CARMIL), excessive production of filiform (thin, thread-like) protrusions around the periphery of intercalating cells correlated with longer intercalation times. This effect could be offset by loss of *unc-73* function, indicating that Rac-GEF activity is necessary for ectopic filiform protrusion production, but that it negatively effects intercalation (Walck-Shannon et al., 2015). Given the relatively strong protrusion defects in *ced-10* and *mig-2* null mutants compared with *unc-73* mutants specifically lacking Rac-GEF activity (Walck-Shannon et al., 2015), however, we hypothesized that additional Rac-GEFs might regulate this pathway. There are two other Rac-GEF orthologs in *C. elegans* that show specificity for CED-10 and MIG-2: VAV-1 (VAV1) and TIAM-1 (Tiam1) (Demarco et al., 2012; Norman et al., 2005; Vettel et al., 2012). In mammals, the function of both VAV1 and Tiam1 have been extensively studied in the immune system. Disrupted expression of both proteins is tightly associated with

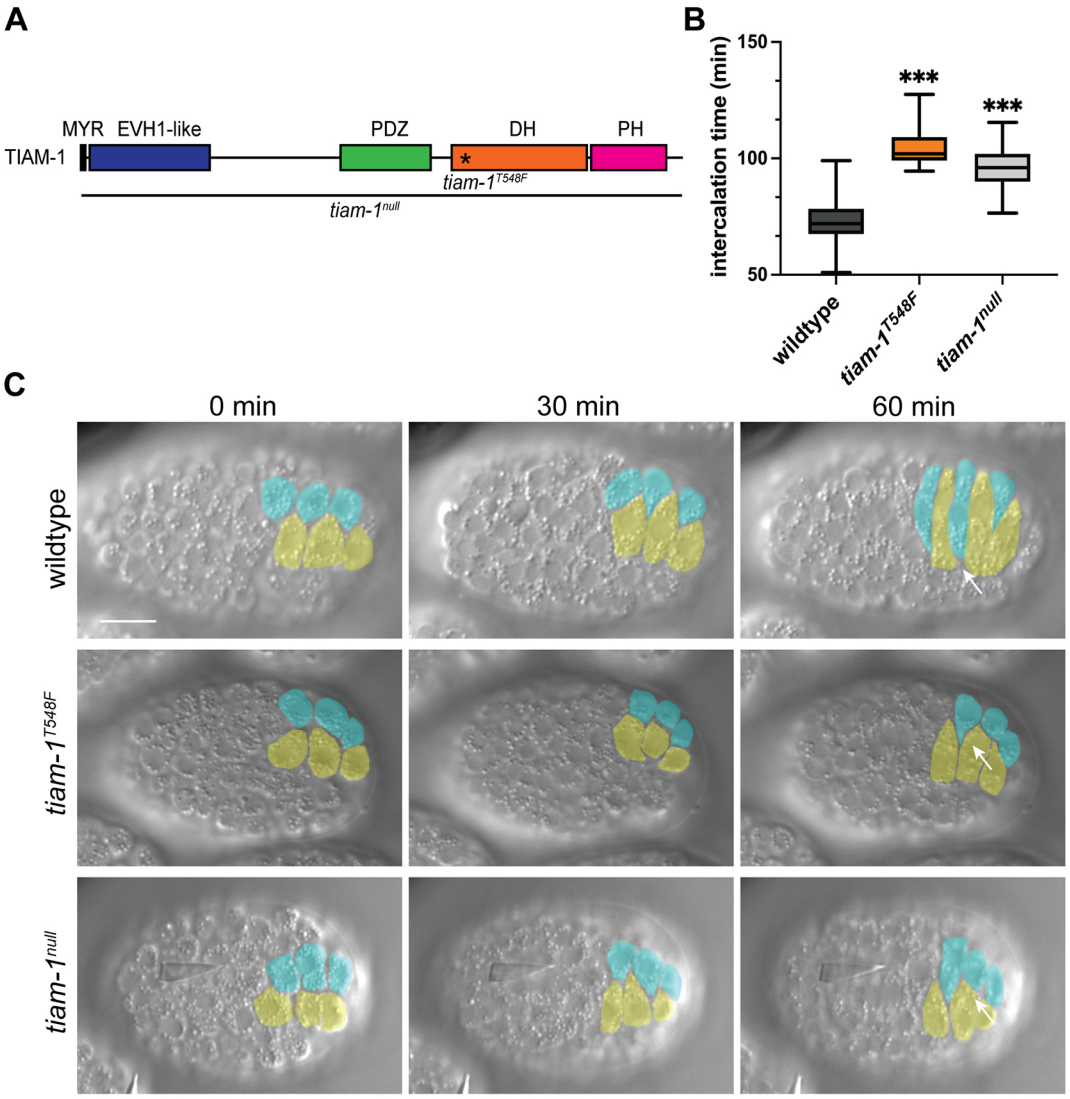

Fig. 1. TIAM-1 is required for normal dorsal intercalation. (A) Protein domain map of *C. elegans* TIAM-1. Domain annotations: MYR, myristoylation site; EVH1-like, Ena/Vasp homology; DH, Dbl homology; PH, pleckstrin homology. The asterisk labels the mutation site of the allele *tiam-1*^{T548F} in the DH domain. The black line labels the deleted region in *tiam-1*^{null}. (B) Intercalation time in *tiam-1*^{T548F} and *tiam-1*^{null} mutants was significantly longer than in wild type. Box plots show the 25–75th percentiles, whiskers show the minimum and maximum values and the median is marked with a line. ***P<0.001, unpaired two-tailed Student's *t*-test. (C) DIC images of dorsal intercalation in wild-type (top), *tiam-1*^{T548F} (middle) and *tiam-1*^{null} (bottom) embryos (dorsal views). Anterior is to the left, posterior to the right; right and left posterior dorsal cells are pseudocolored in cyan and yellow, respectively. White arrows point to the leading edge of right-hand dorsal cells at t=60 min. Cells in wild-type embryos almost made contact with contralateral seam cells, whereas cells in mutants only intercalated halfway. Images are representative of at least 25 embryos from at least eight mounts per genotype. Scale bar: 10 µm.

Journal of Cell Science (2024) 137, jcs261509. doi:10.1242/jcs.261509

uncontrolled cell invasion and metastasis (Bartolomé et al., 2006; Boissier and Huynh-Do, 2014; Gérard et al., 2009; Izumi et al., 2019; Liu et al., 2007; Tybulewicz et al., 2003). Their worm orthologs, VAV-1 and TIAM-1, have been shown to function in axonal outgrowth and guidance (Demarco et al., 2012; Fry et al., 2014; Lin et al., 2022; Malartre et al., 2010; Tang et al., 2019). However, our previous work indicated that knockdown of *vav-1* by RNAi had no effect on dorsal intercalation (Walck-Shannon et al., 2015). We therefore focused on TIAM-1, a multidomain protein including an N-terminal myristoylation domain, an EVH1-like domain, a PDZ domain and a GEF domain composed of Dbl homology (DH) and Pleckstrin homology (PH) subdomains (Fig. 1A) (Demarco et al., 2012).

We first confirmed that *tiam-1* is expressed in the dorsal epidermis. Although we could not detect TIAM-1 using an endogenous mNeonGreen (mNG) knock-in strain or via antibody staining of the tagged protein in this line (Y.Z. and J.H., data not shown), we were able to detect *tiam-1* transcription in dorsal epidermal cells using a *tiam-1* transcriptional reporter strain (Ziel et al., 2009) (Fig. S1). Embryos homozygous for an existing *tiam-1* loss-of-function allele, *tm1556*, as well as embryos from *tiam-1(RNAi)* hermaphrodites displayed delayed completion of dorsal intercalation (Fig. S3A). The gross morphology of the epidermis appeared normal in *tiam-1* loss-of-function embryos, based on differential interference contrast (DIC) movies (Fig. 1C). The intercalation delay was validated by quantifying the intercalation time in both a GEF-dead allele, *tiam-1*^{T548F} (Tang et al., 2019), and a new *tiam-1*^{null} allele we generated, *tiam-1(syb4244),* in which the entire *tiam-1* coding region was eliminated using CRISPR/Cas9 genome editing (Fig. 1B,C).

We also examined potential functional redundancy between UNC-73 and TIAM-1 during dorsal intercalation. *tiam-1(tm1556); unc-73(rh40)* double mutants had a slightly longer intercalation time compared to that of *rh40* homozygotes alone (Fig. S2A). *tiam-1(syb4244);unc-73(RNAi)* null mutants showed a statistically significant difference in number of filiform protrusions as well, especially during early stages of intercalation (Fig. S2B). These results indicate that *tiam-1* is required for normal dorsal intercalation. Moreover, given the defects displayed by *tiam-1*^{T548F} mutants, TIAM-1 appears to function as a Rac-GEF in regulating dorsal intercalation alongside *unc-73*.

TIAM-1 promotes migration in dorsal epidermal cells

We next assessed in detail the effects of abrogating the Rac-GEF activity of TIAM-1 on protrusive behavior of dorsal epidermal cells. In control embryos, dorsal epidermal cells initially generate unpolarized filiform protrusions; shortly thereafter, as cells become wedge shaped and begin to migrate contralaterally, lateral filiform protrusions are retracted and protrusions are concentrated medially (Fig. 2A, left) (Walck-Shannon et al., 2015). We compared this wild-type sequence of behaviors to that displayed by homozygotes for the GEF-dead allele, *tiam-1*^{T548F}. *tiam-1*^{T548F} mutants invariably produced a main medial protrusion; we could not detect a statistically significant difference in the base-to-tip length of the main medial protrusion in *tiam-1*^{T548F} or other *tiam-1* loss-of-function backgrounds (see Fig. S3B). Compared to controls,

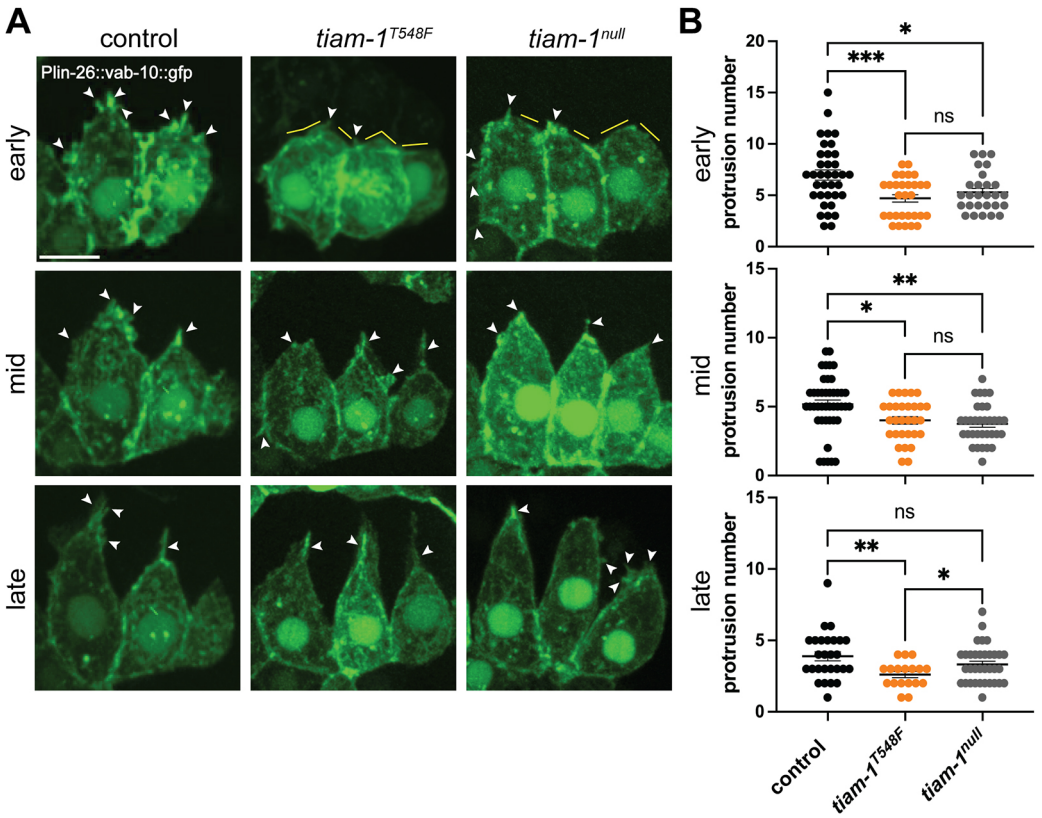

Fig. 2. *tiam-1* loss-of-function mutants generate fewer protrusions during dorsal intercalation. (A) Mosaic expression of an epidermal-specific F-actin reporter (*Plin-26::vab-10::gfp*) shows dynamic protrusions during dorsal intercalation in control (left), *tiam-1*^{T548F} (middle) and *tiam-1*^{null} (right) embryos. White arrowheads indicate protrusions; yellow lines depict the areas lacking protrusions. Scale bar: 5 µm. (B) Quantification of the number of protrusions generated during early, middle and late stages of dorsal intercalation in control and *tiam-1* mutant embryos. Error bars indicate s.e.m. ns, no significant difference; **P*<0.05; ***P*<0.01; ****P*<0.001; one-way ANOVA with Tukey's post hoc test.

Journal of Cell Science (2024) 137, jcs261509. doi:10.1242/jcs.261509

however, *tiam-1*^{T548F} mutants showed significantly fewer filiform protrusions during the entire intercalation process (Fig. 2A, quantified in Fig. 2B), suggesting that the main effect of TIAM-1 is on smaller, filiform protrusions.

We next compared *tiam-1*^{T548F} mutants to homozygotes for a true null allele, *tiam-1*^{null}. Unexpectedly, although *tiam-1*^{null} mutants showed fewer filiform protrusions during the early and middle stages of intercalation, they displayed similar levels of filiform protrusive activity compared to that in controls at later stages, i.e. greater levels of filiform protrusive activity than in *tiam-1*^{T548F} GEF-dead mutants, especially later in dorsal intercalation (Fig. 2A, quantified in Fig. 2B). This result suggested that there might be previously unrecognized inhibitory roles for the N-terminus of TIAM-1.

The N-terminus of TIAM-1 prevents ectopic filiform protrusive activity during dorsal intercalation

Recent work has suggested that the N-terminal domains of TIAM-1 are involved in regulating dendrite development; more specifically, its PDZ domain promotes 4° dendrite branch formation during growth cone morphogenesis (Lin et al., 2022; Tang et al., 2019). We therefore next set out to examine the role of the TIAM-1 N-terminus during dorsal intercalation. Using CRISPR/Cas9, we introduced specific mutations into the *tiam-1* locus, including (1) *tiam-1*$^{\Delta N}$, which removes all N-terminal domains, leaving only the GEF domain intact; (2) *tiam-1*$^{\Delta PDZ}$; and (3) *tiam-1*$^{\Delta PDZ+T548F}$, which introduces the GEF-inactivating mutation into the preceding strain (Fig. 3A).

We first assessed the intercalation phenotypes of the various mutants using DIC microscopy. Mutants all showed significantly increased intercalation time (Fig. S3A). We next crossed the *tiam-1* mutants with an actin reporter strain to visualize F-actin. We could not detect a statistically significant difference in the base-to-tip length of the main medial protrusion in various *tiam-1* loss-of-function backgrounds (Fig. S3B). Although dorsal cells in all mutants eventually produced a main, medially directed lamellipodium, mutant embryos that produced an N-terminally truncated form of TIAM-1 generated significantly more filiform protrusions compared to those in control embryos, specifically during middle to late intercalation, suggesting an inhibitory effect of the N-terminal domains on filiform protrusions at later stages (Fig. 3B, quantified in Fig. 3C). Compared with *tiam-1*^{T548F}, *tiam-1*$^{\Delta PDZ+T548F}$ mutants generated significantly more filiform protrusions during mid-intercalation (Fig. S3C), suggesting that the TIAM-1 N-terminus contributes to filiform protrusive activity via a previously unknown mechanism that is partly independent of the GEF domain. The N terminal domains of TIAM-1 are also required for normal medial polarization of filiform protrusions; *tiam-1* ΔPDZ and ΔN deletion mutants showed significantly reduced polarization compared to that in controls (Fig. S3D). This mispolarization depended in part on TIAM-1 GEF activity, as loss of GEF activity or the GEF domain entirely reverted protrusions to a more normal distribution compared to that in controls (*tiam-1*$^{\Delta PDZ+T548F}$ and *tiam-1*^{null} were not significantly different from controls; Fig. S3D).

The netrin pathway component UNC-5 is a potential upstream regulator of protrusive activity during dorsal intercalation

TIAM-1 has been implicated in netrin-based signaling in growth cones through its association with the netrin receptor, UNC-40 (DCC) (Chan et al., 1996; Demarco et al., 2012; Fearon et al., 1990). We hypothesized that netrin signaling components might similarly act upstream of TIAM-1 during dorsal intercalation. During neurite outgrowth, the netrin pathway can mediate both attraction and repulsion. In the classic case of *C. elegans* growth cone guidance, attractive signaling acts via the extracellular ligand UNC-6 (netrin) and UNC-40. Repulsion often requires the UNC-5 receptor in neurons (Mahadik and Lundquist, 2023; Merz and Culotti, 2000; Norris and Lundquist, 2011; Norris et al., 2014) and other cell types (Su et al., 2000; Ziel and Sherwood, 2010), but classic experiments indicate that *unc-5* can also act independently of *unc-40* (Hedgecock et al., 1990; reviewed in Yam and Charron, 2020). We therefore examined the effects of loss-of-function mutations for *unc-6*, *unc-40* and *unc-5* on intercalation time. Although loss of function of all three loci resulted in a statistically significant increase in intercalation time, the most pronounced effect resulted from loss of *unc-5* function (Fig. 4A). *unc-5* mutants also occasionally displayed mildly aberrant dorsal cell shapes in some embryos.

We next examined localization of UNC-6, UNC-40 and UNC-5 using available knock-in strains (Jayadev et al., 2022). UNC-6 was expressed predominantly ventrally, without detectable signal in the epidermis near or shortly after the time dorsal intercalation occurs (Fig. S4A). UNC-40 was expressed at low levels in dorsal epidermal cells throughout dorsal intercalation, with stronger expression in ventral neuroblasts, including prominent foci (Fig. S4B). In contrast, UNC-5 showed strong expression only in the dorsal epidermis (Fig. S4C). UNC-5 was initially visible in cytosolic granules, which we assume are secretory vesicles. As dorsal intercalation progressed, UNC-5 accumulated at the lateral membranes of dorsal epidermal cells. Strikingly, UNC-5 showed an increased accumulation at the lateral edges of dorsal cells (Fig. 4B,C). The localization pattern of UNC-5 and effects on intercalation time following loss of *unc-5* function make *unc-5* a promising upstream candidate involved in the previously unreported inhibitory regulatory function of TIAM-1, and so we focused on it for further analysis.

Our previous work had shown that dorsal epidermal cells quickly become polarized at the onset of dorsal intercalation (Walck-Shannon et al., 2015). As the presence of UNC-5 is often associated with growth cone repulsion (Keleman and Dickson, 2001; Mahadik and Lundquist, 2023; Norris and Lundquist, 2011), the localization of UNC-5 in dorsal epidermal cells suggests a simple model: UNC-5 inhibits filiform protrusive activity at membrane surfaces where it is expressed, biasing protrusion towards the leading edge. Consistent with this model, dorsal epidermal cells in embryos homozygous for a nonsense allele of *unc-5(e152)* exhibited ectopic filiform protrusions (Fig. 4D, quantified in Fig. 4E) that largely lacked polarity (Fig. 4F). In contrast, *unc-6(RNAi)* and *unc-40(RNAi)* embryos showed no defects in protrusion formation (Fig. S4D), despite loss of detectable mNG signal (Fig. S4E). Several previous studies uncovered UNC-40-independent functions for UNC-5, based on comparison of the severity of defects between *unc-5* and *unc-40* mutants (Killeen et al., 2002; MacNeil et al., 2009; Mahadik and Lundquist, 2023). These results, combined with our analysis, suggest that UNC-5 likely has an UNC-40-independent function in inhibiting protrusions during dorsal intercalation.

Considering the similarity of defects shown in *unc-5(e152)* and *tiam-1* N-terminal mutants (ectopic filiform protrusions and loss of medially polarized protrusions at late stages of intercalation) we next assessed whether there was any connection between UNC-5 and TIAM-1 function during dorsal intercalation. RNAi

Journal of Cell Science (2024) 137, jcs261509. doi:10.1242/jcs.261509

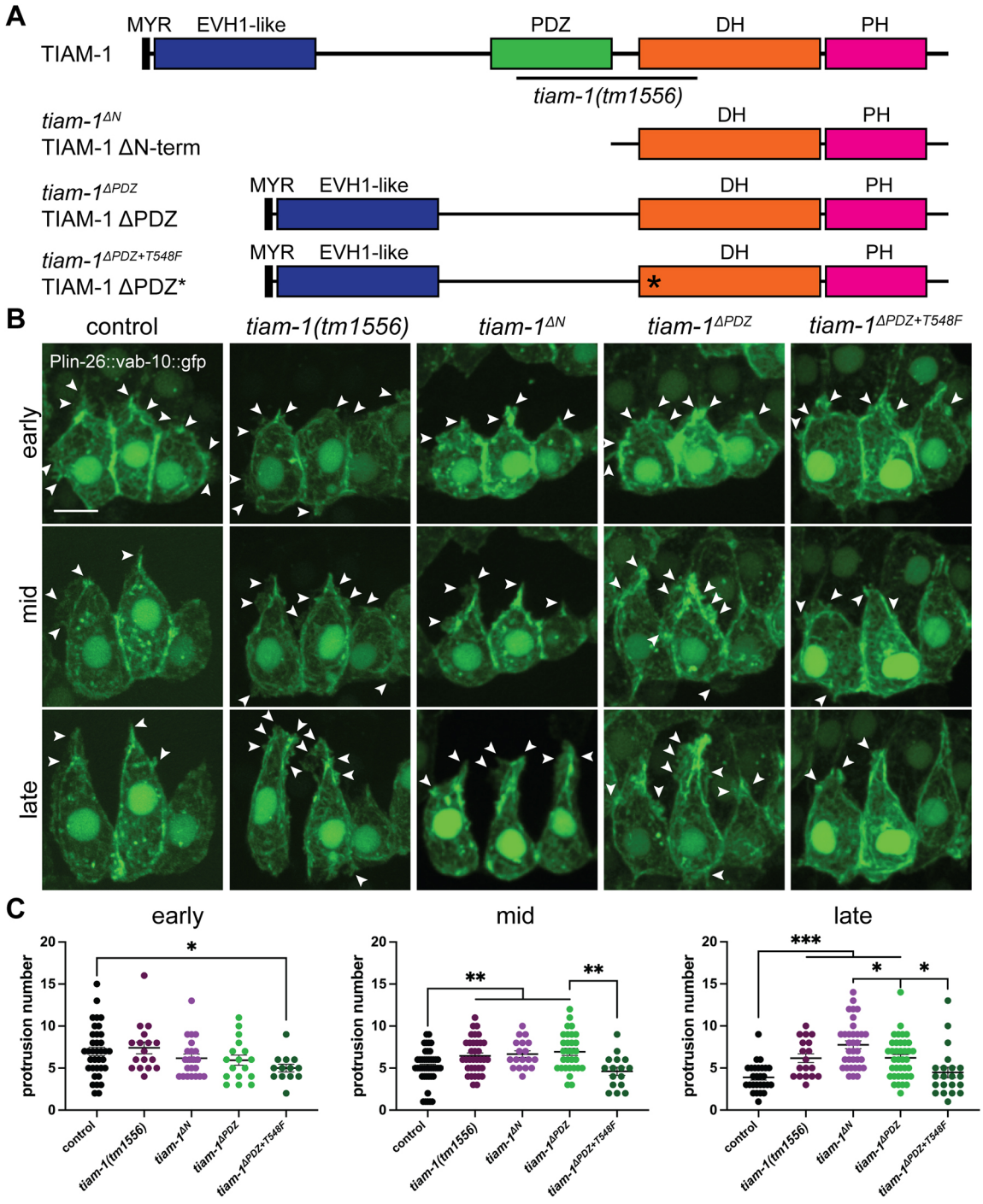

Fig. 3. TIAM-1 N-terminal deletions lead to ectopic and unpolarized protrusions. (A) Domain maps of TIAM-1 and N-terminal deletions relevant to this study. *tiam-1*$^{\Delta N}$, truncated protein removing all N-terminal domains, leaving only the GEF domain; *tiam-1*$^{\Delta PDZ}$, truncated protein removing only the PDZ domain; *tiam-1*$^{\Delta PDZ+T548F}$, truncated protein removing the PDZ domain and containing the T548F point mutation (asterisk). The black line indicates the lesion in *tiam-1(tm1556)*. (B) Compared to controls, *tiam-1* N-terminal deletion mutants displayed ectopic filiform protrusions, which could be partially ameliorated by eliminating the GEF activity of TIAM-1 (*tiam-1*$^{\Delta PDZ+T548F}$). White arrowheads indicate protrusions. Scale bar: 5 µm. For analysis of orientation of filiform protrusions, see Fig. S1D. (C) Quantification of the number of protrusions generated during early, middle and late stages of dorsal intercalation in control and *tiam-1* N-terminal deletion mutants. Error bars indicate s.e.m. *P<0.05; **P<0.01; ***P<0.001; one-way ANOVA with Tukey's post hoc test.

knockdown of *tiam-1* in *unc-5(e152)* mutants rescued the ectopic protrusions observed in *unc-5(e152)* mutants alone such that their number and distribution were statistically indistinguishable from those of controls (Fig. 4E,F), suggesting that UNC-5 is involved in regulating Rac-dependent filiform protrusions during dorsal intercalation in part via TIAM-1.

The cortical localization of UNC-5 to lateral membranes in dorsal epidermal cells is intriguing and presumably results from contact-mediated or other signaling events. Mechanisms of UNC-5 localization have not been extensively investigated. One study implicates UNC-51 (a serine-threonine kinase) and the RUN domain protein UNC-14 in normal localization of UNC-5 in neurons (Ogura

Journal of Cell Science (2024) 137, jcs261509. doi:10.1242/jcs.261509

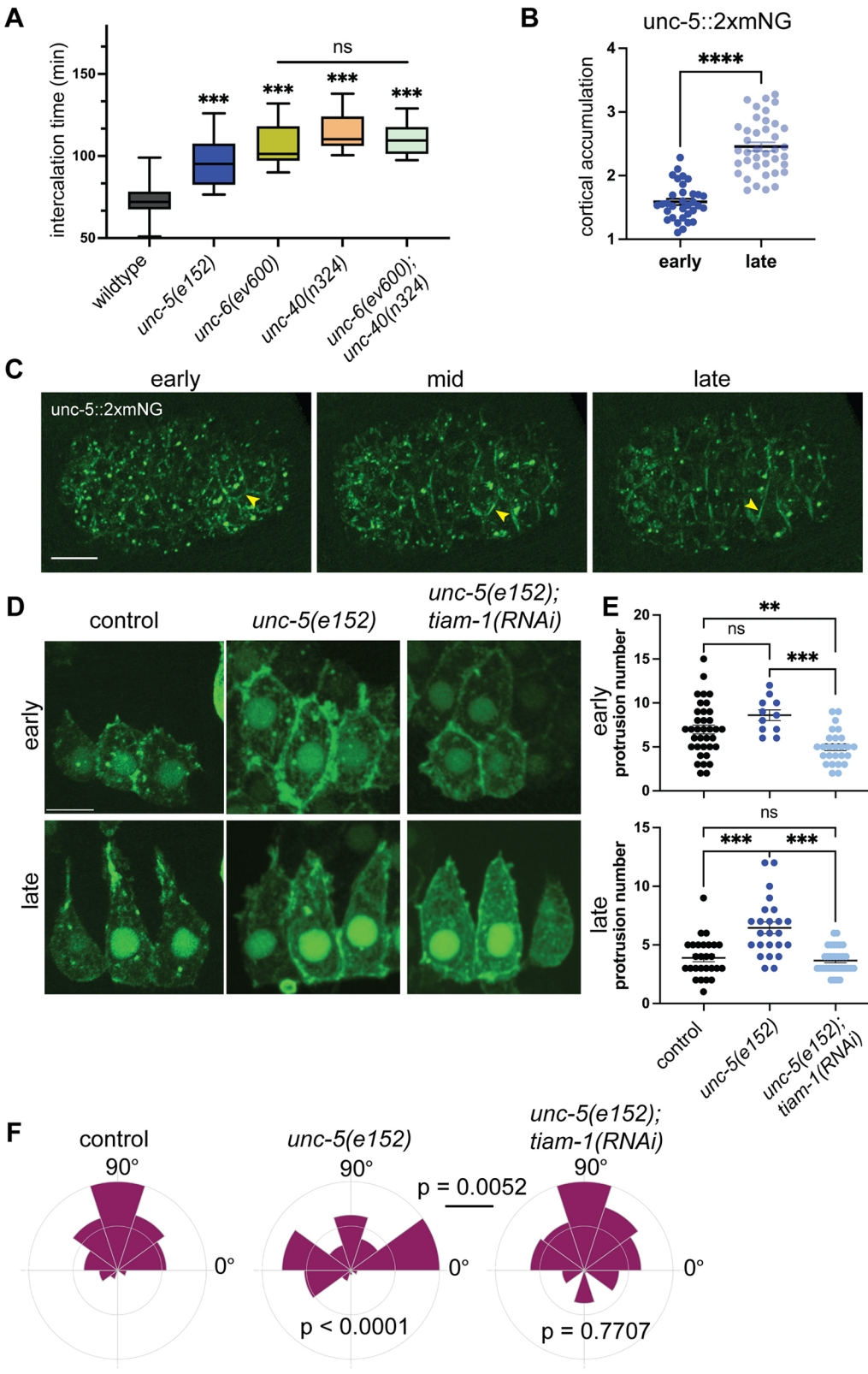

Fig. 4. See next page for legend.

and Goshima, 2006). These two proteins are involved in autophagy in other contexts, suggesting that these proteins regulate trafficking of UNC-5 to the membrane. Whether such trafficking is spatially polarized is not clear and is an interesting area for future study.

In summary, our results indicate that TIAM-1 acts as a Rac-GEF in promoting protrusive activity during dorsal intercalation. Its N-terminus also appears to exert an inhibitory effect on filiform protrusions independent of its GEF activity, specifically during

Fig. 4. UNC-5 depletion leads to ectopic protrusive activity. (A) Mutants in netrin pathway components *unc-5*, *unc-6* and *unc-40* displayed delayed completion of dorsal intercalation. Box plots show the 25–75th percentiles, whiskers show the minimum and maximum, and the median is marked with a line. ns, no significant difference; ***P<0.001; unpaired two-tailed Student's *t*-test. (B) UNC-5 became peripherally enriched as dorsal intercalation progressed. Error bars indicate s.e.m. ****P<0.0001; unpaired two-tailed Student's *t*-test. (C) Expression pattern of UNC-5::2×mNG during dorsal intercalation. Yellow arrowheads indicate lateral boundaries of intercalating dorsal cells. Scale bar: 10 µm. (D) Dorsal epidermal cells in a nonsense mutant [*unc-5(e152)*] exhibit ectopic filiform protrusions during late intercalation that are partially suppressed via *tiam-1* knockdown. White arrowheads indicate protrusions. Scale bar: 5 µm. (E) Quantification of the number of protrusions generated during early, middle and late stages of dorsal intercalation in wildtype and *unc-5(e152)* mutants. Error bars indicate s.e.m. ns, no significant difference; **P<0.01; ***P<0.001; one-way ANOVA with Tukey's post hoc test. (F) Protrusions showed reduced medial polarization in *unc-5(e152)* mutants, which could be partially rescued by RNAi knockdown of *tiam-1*. Rose plots of the angle of protrusion relative to the cell centroid at the late stage of dorsal intercalation. Annotated P-values were calculated using the Mardia–Watson–Wheeler test. P-values below the plots compare mutants with wildtype; the P-value above the black line compares *unc-5(e152)* with *unc-5(e152);tiam-1(RNAi)*.

middle to late stages of intercalation. Finally, UNC-5 might act upstream of TIAM-1 during dorsal intercalation independent of UNC-6 and UNC-40, establishing a previously unreported role for this highly conserved receptor in regulating filiform protrusions during directed cell rearrangement.

MATERIALS AND METHODS

Strains

Caenorhabditis elegans strains were maintained on standard nematode growth medium plates seeded with OP50 *Escherichia coli* at 20°C (Brenner, 1974). Bristol N2 was used as the wild type. Details of strains used in this study can be found in Table S1.

CRISPR/Cas9 genome editing

All novel mutant alleles with the '*jc##*' designation were generated via plasmid-based CRISPR/Cas9 editing (Dickinson et al., 2015) using repair templates cloned by SapTrap cloning (Schwartz and Jorgensen, 2016). Both deletion mutations (*syb4155* and *syb4244* alleles) were generated by SunyBiotech (Fujian, China). Guides, homology arm primers and single-stranded repair templates for all CRISPR/Cas9 editing can be found in Table S2.

RNA interference

Feeding RNAi was performed as described by transferring L4 worms to plates seeded with *E. coli* expressing double-stranded (ds)RNA from the relevant target gene or L4440 (control) vectors overnight (Walston et al., 2004). The following day, embryos were dissected from RNAi-treated hermaphrodites and mounted for imaging.

Injection RNAi was performed as described previously (Walston et al., 2004). dsRNA was generated using the T7 Megascript kit (Invitrogen). dsRNA was injected at a concentration of 2 µg/µl in nuclease-free water. L4 worms were injected and aged overnight before embryos were dissected from mature adults for imaging. The templates for C11D9.1 (*tiam-1*), F55C7.7 (*unc-73*), T19B4.7 (*unc-40*), F41C6.1 (*unc-6*) and control RNAi were obtained from the Ahringer feeding library (Kamath et al., 2003).

DIC imaging

Four-dimensional DIC movies were collected on either a Nikon Optiphot-2 microscope connected to a QiCAM camera (QImaging) or an Olympus BX50 microscope connected to a Scion CFW-1512M camera using Micro-Manager software (v1.4) (Edelstein et al., 2010, 2014). All embryos were mounted on 10% agar pads in M9 solution as previously described (Raich et al., 1999).

Confocal imaging

Embryos were dissected from adult hermaphrodites and mounted onto 10% agar pads in M9 solution and imaged. For fluorescence imaging of actin reporter lines, a Dragonfly 500 spinning disc confocal microscope (Andor), mounted on a Leica DMi8 microscope equipped with a Zyla camera and controlled by Fusion software (Andor), was used to collect images with 0.3 µm slices with a 100×/1.3 NA oil immersion Leica objective at 20°C. Movies were acquired either over a period of 30 min at 20 s intervals or over a period of 60 min at 1 min intervals. For imaging of *unc-6(RNAi)* and *unc-40(RNAi)*, the same system was used; images of mNG knock-in strains were collected at 90 s intervals for 60 min using a 63× glycerol immersion Leica objective at 20°C. Focal planes totaling 6 µm in depth were acquired and projected to assess knockdown. For imaging of the *tiam-1* transcriptional reporter line, the same system was used, except that an Andor iXon EMCCD camera was used for acquisition to increase sensitivity. Movies were acquired over a period of 120 min at 3 min intervals.

Quantification of dorsal intercalation time

Quantification of intercalation time was performed from DIC movies of embryos mounted on agar pads. For this study, we defined intercalation time as the time between terminal epidermal divisions (specifically, the divisions of Cpaaa and Cpaap) and when cells met contralateral seam cells. At least 20 embryos from at least eight mounts were analyzed per genotype.

Quantification of protrusions

Protrusions were quantified from maximum-intensity projections of 13 *z*-stacks of F-actin reporter expression as described above. Quantification was performed essentially as described previously (Walck-Shannon et al., 2015). In order to avoid bias in assuming which protrusions were functionally important for migration, protrusion number was obtained by counting aggregations of F-actin reporter signal extending at least 0.2 µm from the cell body. Angles were obtained by comparing the protrusion extension directions relative to the anterior–posterior axis of the embryo in ImageJ. At least ten cells from at least five embryos were analyzed per genotype. We designated cells as 'early' if they were in the process of polarizing into a wedge shape, 'mid' if the cell tips were ≤2 µm past the dorsal midline, and 'late' if the cell tips were ≤2 µm from the contralateral seam cells. The main medial protrusion length in mid-intercalation-stage embryos was determined from actin reporter movies by manually drawing a line selection from the base of the protrusion to its tip using Fiji (https://fiji.sc).

Statistical analysis

Data from control and experimental groups were compared using one-way ANOVA with Tukey's post hoc testing to assess significance between individual groups using Prism (GraphPad). Protrusion angle-related data were compared using the Mardia–Watson–Wheeler test in R using the Circular package (https://CRAN.R-project.org/package=circular).

Acknowledgements

The strain *tiam-1*^{T548F} was provided by the Bülow laboratory. Some strains were provided by the *Caenorhabditis* Genetics Center, which is funded by the National Institutes of Health Office of Research Infrastructure Programs (P40 OD010440).

Competing interests

The authors declare no competing or financial interests.

Author contributions

Conceptualization: Y.Z., J.H.; Methodology: Y.Z.; Validation: Z.T., M.T.; Formal analysis: Y.Z., Z.T.; Investigation: Y.Z., Z.T., M.T.; Resources: J.H.; Writing - original draft: Y.Z.; Writing - review & editing: Y.Z., Z.T., J.H.; Visualization: Y.Z., Z.T.; Supervision: J.H.; Project administration: J.H.; Funding acquisition: J.H.

Funding

This work was supported by grants R01GM127687 and R35GM145312 from the National Institutes of Health awarded to J.H. Deposited in PMC for release after 12 months.

Data availability

All relevant data can be found within the article and its supplementary information.

Peer review history
The peer review history is available online at https://journals.biologists.com/jcs/lookup/doi/10.1242/jcs.261509.reviewer-comments.pdf

References

Bartolomé, R. A., Molina-Ortiz, I., Samaniego, R., Sánchez-Mateos, P., Bustelo, X. R. and Teixidó, J. (2006). Activation of Vav/Rho GTPase signaling by CXCL12 controls membrane-type matrix metalloproteinase–dependent melanoma cell invasion. *Cancer Res.* **66**, 248-258. doi:10.1158/0008-5472.CAN-05-2489

Bertet, C., Sulak, L. and Lecuit, T. (2004). Myosin-dependent junction remodelling controls planar cell intercalation and axis elongation. *Nature* **429**, 667-671. doi:10.1038/nature02590

Boissier, P. and Huynh-Do, U. (2014). The guanine nucleotide exchange factor Tiam1: a Janus-faced molecule in cellular signaling. *Cell. Signal.* **26**, 483-491. doi:10.1016/j.cellsig.2013.11.034

Brenner, S. (1974). The genetics of Caenorhabditis elegans. *Genetics* **77**, 71-94. doi:10.1093/genetics/77.1.71

Chan, S.-Y., Zheng, H., Su, M.-W., Wilk, R., Killeen, M., Hedgecock, E. and Culotti, J. (1996). UNC-40, a C. elegans homolog of DCC (Deleted in Colorectal Cancer), is required in motile cells responding to UNC-6 netrin cues. *Cell* **87**, 187-195. doi:10.1016/S0092-8674(00)81337-9

Demarco, R. S., Struckhoff, E. C. and Lundquist, E. A. (2012). The Rac GTP exchange factor TIAM-1 acts with CDC-42 and the guidance receptor UNC-40/DCC in neuronal protrusion and axon guidance. *PLoS Genet.* **8**, e1002665. doi:10.1371/journal.pgen.1002665

Dickinson, D. J., Pani, A. M., Heppert, J. K., Higgins, C. D. and Goldstein, B. (2015). Streamlined genome engineering with a self-excising drug selection cassette. *Genetics* **200**, 1035-1049. doi:10.1534/genetics.115.178335

Driver, E. C., Northrop, A. and Kelley, M. W. (2017). Cell migration, intercalation and growth regulate mammalian cochlear extension. *Development* **144**, 3766-3776. doi:10.1242/dev.151761

Edelstein, A., Amodaj, N., Hoover, K., Vale, R. and Stuurman, N. (2010). Computer control of microscopes using microManager. *Curr. Protoc. Mol. Biol.* **Chapter 14**, Unit14 20. doi:10.1002/0471142727.mb1420s92

Edelstein, A. D., Tsuchida, M. A., Amodaj, N., Pinkard, H., Vale, R. D. and Stuurman, N. (2014). Advanced methods of microscope control using μManager software. *J. Biol. Methods* **1**, e10. doi:10.14440/jbm.2014.36

Fearon, E. R., Cho, K. R., Nigro, J. M., Kern, S. E., Simons, J. W., Ruppert, J. M., Preisinger, A. C., Thomas, G., Kinzler, K. W. and Vogelstein, B. (1990). Identification of a chromosome 18q gene that is altered in colorectal cancers. *Science* **247**, 49-56. doi:10.1126/science.2294591

Fry, A. L., Laboy, J. T. and Norman, K. R. (2014). VAV-1 acts in a single interneuron to inhibit motor circuit activity in Caenorhabditis elegans. *Nat. Commun.* **5**, 5579. doi:10.1038/ncomms6579

Gérard, A., van der Kammen, R. A., Janssen, H., Ellenbroek, S. I. and Collard, J. G. (2009). The Rac activator Tiam1 controls efficient T-cell trafficking and route of transendothelial migration. *Blood* **113**, 6138-6147. doi:10.1182/blood-2008-07-167668

Hedgecock, E. M., Culotti, J. G. and Hall, D. H. (1990). The unc-5, unc-6, and unc-40 genes guide circumferential migrations of pioneer axons and mesodermal cells on the epidermis in C. elegans. *Neuron* **4**, 61-85. doi:10.1016/0896-6273(90)90444-K

Huebner, R. J. and Wallingford, J. B. (2018). Coming to consensus: a unifying model emerges for convergent extension. *Dev. Cell* **46**, 389-396. doi:10.1016/j.devcel.2018.08.003

Izumi, D., Toden, S., Ureta, E., Ishimoto, T., Baba, H. and Goel, A. (2019). TIAM1 promotes chemoresistance and tumor invasiveness in colorectal cancer. *Cell Death Dis.* **10**, 267. doi:10.1038/s41419-019-1493-5

Jayadev, R., Morais, M. R., Ellingford, J. M., Srinivasan, S., Naylor, R. W., Lawless, C., Li, A. S., Ingham, J. F., Hastie, E. and Chi, Q. (2022). A basement membrane discovery pipeline uncovers network complexity, regulators, and human disease associations. *Sci. Adv.* **8**, eabn2265. doi:10.1126/sciadv.abn2265

Kamath, R. S., Fraser, A. G., Dong, Y., Poulin, G., Durbin, R., Gotta, M., Kanapin, A., Le Bot, N., Moreno, S. and Sohrmann, M. (2003). Systematic functional analysis of the Caenorhabditis elegans genome using RNAi. *Nature* **421**, 231-237. doi:10.1038/nature01278

Keleman, K. and Dickson, B. J. (2001). Short-and long-range repulsion by the Drosophila Unc5 netrin receptor. *Neuron* **32**, 605-617. doi:10.1016/S0896-6273(01)00505-0

Killeen, M., Tong, J., Krizus, A., Steven, R., Scott, I., Pawson, T. and Culotti, J. (2002). UNC-5 function requires phosphorylation of cytoplasmic tyrosine 482, but its UNC-40-independent functions also require a region between the ZU-5 and death domains. *Dev. Biol.* **251**, 348-366. doi:10.1006/dbio.2002.0825

Kong, D., Wolf, F. and Großhans, J. (2017). Forces directing germ-band extension in Drosophila embryos. *Mech. Dev.* **144**, 11-22. doi:10.1016/j.mod.2016.12.001

Lin, C.-H., Chen, Y.-C., Chan, S.-P. and Ou, C.-Y. (2022). TIAM-1 differentially regulates dendritic and axonal microtubule organization in patterning neuronal development through its multiple domains. *PLoS Genet.* **18**, e1010454. doi:10.1371/journal.pgen.1010454

Liu, L., Zhao, L., Zhang, Y., Zhang, Q. and Ding, Y. (2007). Proteomic analysis of Tiam1–mediated metastasis in colorectal cancer. *Cell Biol. Int.* **31**, 805-814. doi:10.1016/j.cellbi.2007.01.014

MacNeil, L. T., Hardy, W. R., Pawson, T., Wrana, J. L. and Culotti, J. G. (2009). UNC-129 regulates the balance between UNC-40 dependent and independent UNC-5 signaling pathways. *Nat. Neurosci.* **12**, 150-155. doi:10.1038/nn.2256

Mahadik, S. S. and Lundquist, E. A. (2023). A short isoform of the UNC-6/Netrin receptor UNC-5 is required for growth cone polarity and robust growth cone protrusion in Caenorhabditis elegans. *Front. Cell. Dev. Biol.* **11**, 1240994. doi:10.3389/fcell.2023.1240994

Malartre, M., Ayaz, D., Amador, F. F. and Martín-Bermudo, M. D. (2010). The guanine exchange factor vav controls axon growth and guidance during Drosophila development. *J. Neurosci.* **30**, 2257-2267. doi:10.1523/JNEUROSCI.1820-09.2010

Merz, D. C. and Culotti, J. G. (2000). Genetic analysis of growth cone migrations in Caenorhabditis elegans. *J. Neurobiol.* **44**, 281-288. doi:10.1002/1097-4695(200008)44:2<281::AID-NEU16>3.0.CO;2-4

Munro, E. M. and Odell, G. (2002a). Morphogenetic pattern formation during ascidian notochord formation is regulative and highly robust. *Development* **129**, 1-12. doi:10.1242/dev.129.1.1

Munro, E. M. and Odell, G. M. (2002b). Polarized basolateral cell motility underlies invagination and convergent extension of the ascidian notochord. *Development* **129**, 13-24. doi:10.1242/dev.129.1.13

Nikolopoulou, E., Galea, G. L., Rolo, A., Greene, N. D. and Copp, A. J. (2017). Neural tube closure: cellular, molecular and biomechanical mechanisms. *Development* **144**, 552-566. doi:10.1242/dev.145904

Norman, K. R., Fazzio, R. T., Mellem, J. E., Espelt, M. V., Strange, K., Beckerle, M. C. and Maricq, A. V. (2005). The Rho/Rac-family guanine nucleotide exchange factor VAV-1 regulates rhythmic behaviors in C. elegans. *Cell* **123**, 119-132. doi:10.1016/j.cell.2005.08.001

Norris, A. D. and Lundquist, E. A. (2011). UNC-6/netrin and its receptors UNC-5 and UNC-40/DCC modulate growth cone protrusion in vivo in C. elegans. *Development* **138**, 4433-4442. doi:10.1242/dev.068841

Norris, A. D., Sundararajan, L., Morgan, D. E., Roberts, Z. J. and Lundquist, E. A. (2014). The UNC-6/Netrin receptors UNC-40/DCC and UNC-5 inhibit growth cone filopodial protrusion via UNC-73/Trio, Rac-like GTPases and UNC-33/CRMP. *Development* **141**, 4395-4405. doi:10.1242/dev.110437

Ogura, K. and Goshima, Y. (2006). The autophagy-related kinase UNC-51 and its binding partner UNC-14 regulate the subcellular localization of the Netrin receptor UNC-5 in Caenorhabditis elegans. *Development* **133**, 3441-3450. doi:10.1242/dev.02503

Patel, F. B., Bernadskaya, Y. Y., Chen, E., Jobanputra, A., Pooladi, Z., Freeman, K. L., Gally, C., Mohler, W. A. and Soto, M. C. (2008). The WAVE/SCAR complex promotes polarized cell movements and actin enrichment in epithelia during C. elegans embryogenesis. *Dev. Biol.* **324**, 297-309. doi:10.1016/j.ydbio.2008.09.023

Pilot, F. and Lecuit, T. (2005). Compartmentalized morphogenesis in epithelia: from cell to tissue shape. *Dev. Dyn.* **232**, 685-694. doi:10.1002/dvdy.20334

Raich, W. B., Agbunag, C. and Hardin, J. (1999). Rapid epithelial-sheet sealing in the Caenorhabditis elegans embryo requires cadherin-dependent filopodial priming. *Curr. Biol.* **9**, 1139-1146. doi:10.1016/S0960-9822(00)80015-9

Schwartz, M. L. and Jorgensen, E. M. (2016). SapTrap, a toolkit for high-throughput CRISPR/Cas9 gene modification in Caenorhabditis elegans. *Genetics* **202**, 1277-1288. doi:10.1534/genetics.115.184275

Solnica-Krezel, L. and Sepich, D. S. (2012). Gastrulation: making and shaping germ layers. *Annu. Rev. Cell Dev. Biol.* **28**, 687-717. doi:10.1146/annurev-cellbio-092910-154043

Su, M.-W., Merz, D. C., Killeen, M. T., Zhou, Y., Zheng, H., Kramer, J. M., Hedgecock, E. M. and Culotti, J. G. (2000). Regulation of the UNC-5 netrin receptor initiates the first reorientation of migrating distal tip cells in Caenorhabditis elegans. *Development* **127**, 585-594. doi:10.1242/dev.127.3.585

Sutherland, A., Keller, R. and Lesko, A. (2020). Convergent extension in mammalian morphogenesis. In *Seminars in Cell & Developmental Biology*, Vol. 100, pp. 199-211. Elsevier. doi:10.1016/j.semcdb.2019.11.002

Tang, L. T., Diaz-Balzac, C. A., Rahman, M., Ramirez-Suarez, N. J., Salzberg, Y., Lazaro-Pena, M. I. and Bülow, H. E. (2019). TIAM-1/GEF can shape somatosensory dendrites independently of its GEF activity by regulating F-actin localization. *Elife* **8**, e38949. doi:10.7554/eLife.38949

Tybulewicz, V. L., Ardouin, L., Prisco, A. and Reynolds, L. F. (2003). Vav1: a key signal transducer downstream of the TCR. *Immunol. Rev.* **192**, 42-52. doi:10.1034/j.1600-065X.2003.00032.x

Vettel, C., Wittig, K., Vogt, A., Wuertz, C. M., El-Armouche, A., Lutz, S. and Wieland, T. (2012). A novel player in cellular hypertrophy: Giβγ/PI3K-dependent activation of the RacGEF TIAM-1 is required for α1-adrenoceptor induced hypertrophy in neonatal rat cardiomyocytes. *J. Mol. Cell. Cardiol.* **53**, 165-175. doi:10.1016/j.yjmcc.2012.04.015

Walck-Shannon, E. and Hardin, J. (2014). Cell intercalation from top to bottom. *Nat. Rev. Mol. Cell Biol.* **15**, 34-48. doi:10.1038/nrm3723

Walck-Shannon, E., Reiner, D. and Hardin, J. (2015). Polarized Rac-dependent protrusions drive epithelial intercalation in the embryonic epidermis of C. elegans. *Development* **142**, 3549-3560. doi:10.1242/dev.127597

Walston, T., Tuskey, C., Edgar, L., Hawkins, N., Ellis, G., Bowerman, B., Wood, W. and Hardin, J. (2004). Multiple Wnt signaling pathways converge to orient the mitotic spindle in early C. elegans embryos. *Dev. Cell* **7**, 831-841. doi:10.1016/j.devcel.2004.10.008

Williams-Masson, E. M., Heid, P., Lavin, C. and Hardin, J. (1998). The cellular mechanism of epithelial rearrangement during morphogenesis of the Caenorhabditis elegans dorsal hypodermis. *Dev. Biol.* **204**, 263-276. doi:10.1006/dbio.1998.9048

Williams, M., Yen, W., Lu, X. and Sutherland, A. (2014). Distinct apical and basolateral mechanisms drive planar cell polarity-dependent convergent extension of the mouse neural plate. *Dev. Cell* **29**, 34-46. doi:10.1016/j.devcel.2014.02.007

Yam, P. T. and Charron, F. (2020). Chapter 8 - Nonconventional axon guidance cues: Hedgehog, TGF-β/BMP, and Wnts in axon guidance. In *Cellular Migration and Formation of Axons and Dendrites* (ed. J. Rubenstein, B. Chen, A. Kolodkin, P. Rakic, K. Y. Kwan and E. Anton), pp. 175-199. New York, NY: Academic Press. doi:10.1016/B978-0-12-814407-7.00008-0

Ziel, J. W. and Sherwood, D. R. (2010). Roles for netrin signaling outside of axon guidance: a view from the worm. *Dev. Dyn.* **239**, 1296-1305. doi:10.1002/dvdy.22225

Ziel, J. W., Hagedorn, E. J., Audhya, A. and Sherwood, D. R. (2009). UNC-6 (netrin) orients the invasive membrane of the anchor cell in C. elegans. *Nat. Cell Biol.* **11**, 183-189. doi:10.1038/ncb1825

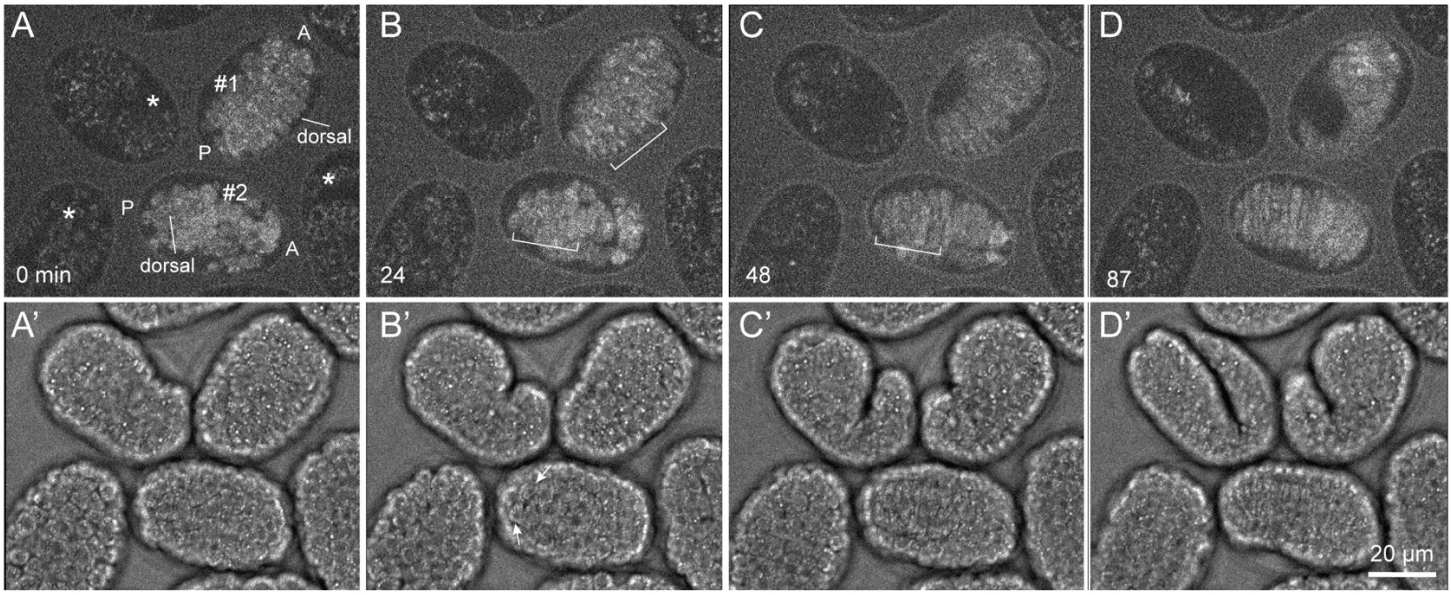

Fig. S1. A *tiam-1* transcriptional reporter is expressed prior to and during dorsal intercalation. Frames from a 4d movie of a representative field of transgenic embryos expressing a *tiam-1* transcriptional reporter. Two embryos fully in the field of view express a *Ptiam-1::gfp* extrachromosomal array (labeled #1 and #2). One embryo fully in the field of view and two partially in the field of view do not express the array (asterisks). (A-D) Confocal images; (A'-D') DIC images. Elapsed time relative to the first frame is indicated in min. Dorsal-up embryos expressing the array are indicated. A = anterior; P = posterior. Arrows in B' indicate two posterior dorsal cells that have begun to wedge. Brackets in B and C indicate the dorsal array during and after intercalation.

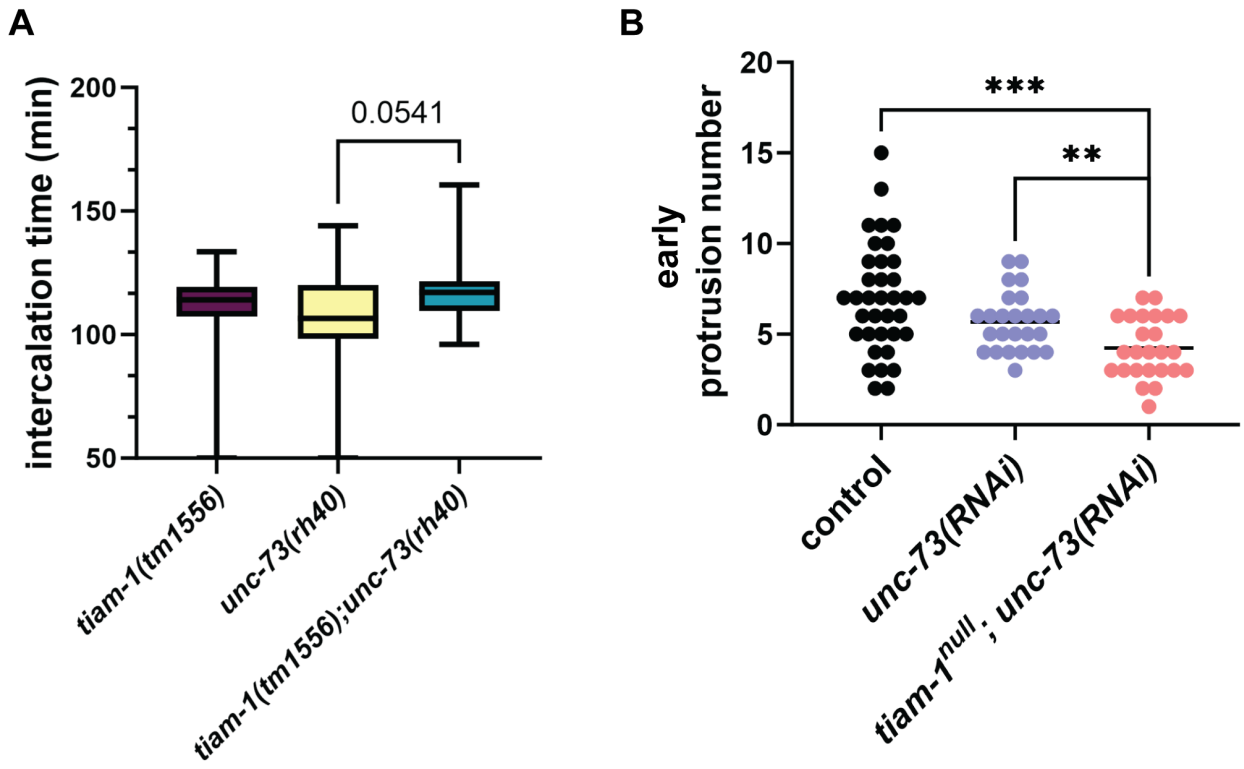

Fig. S2. UNC-73 functions alongside TIAM-1 to promote filiform protrusions

(A) Intercalation times of *tiam-1(tm1556)*, *unc-73(rh40) and tiam-1(tm1556);unc-73(rh40)* embryos. Intercalation time in *tiam-1(tm1556);unc-73(rh40)* mutants is compared to *unc-73(rh40)* mutants alone is p =0.0541; unpaired Student's T test.

(B) Quantification of the number of protrusions generated during the early stage of dorsal intercalation in control, *unc-73(RNAi)* and *tiam-1^{null};unc-73(RNAi)* embryos. Error bars indicate s.e.m. ***, p < 0.001; **, p < 0.01; one-way ANOVA.

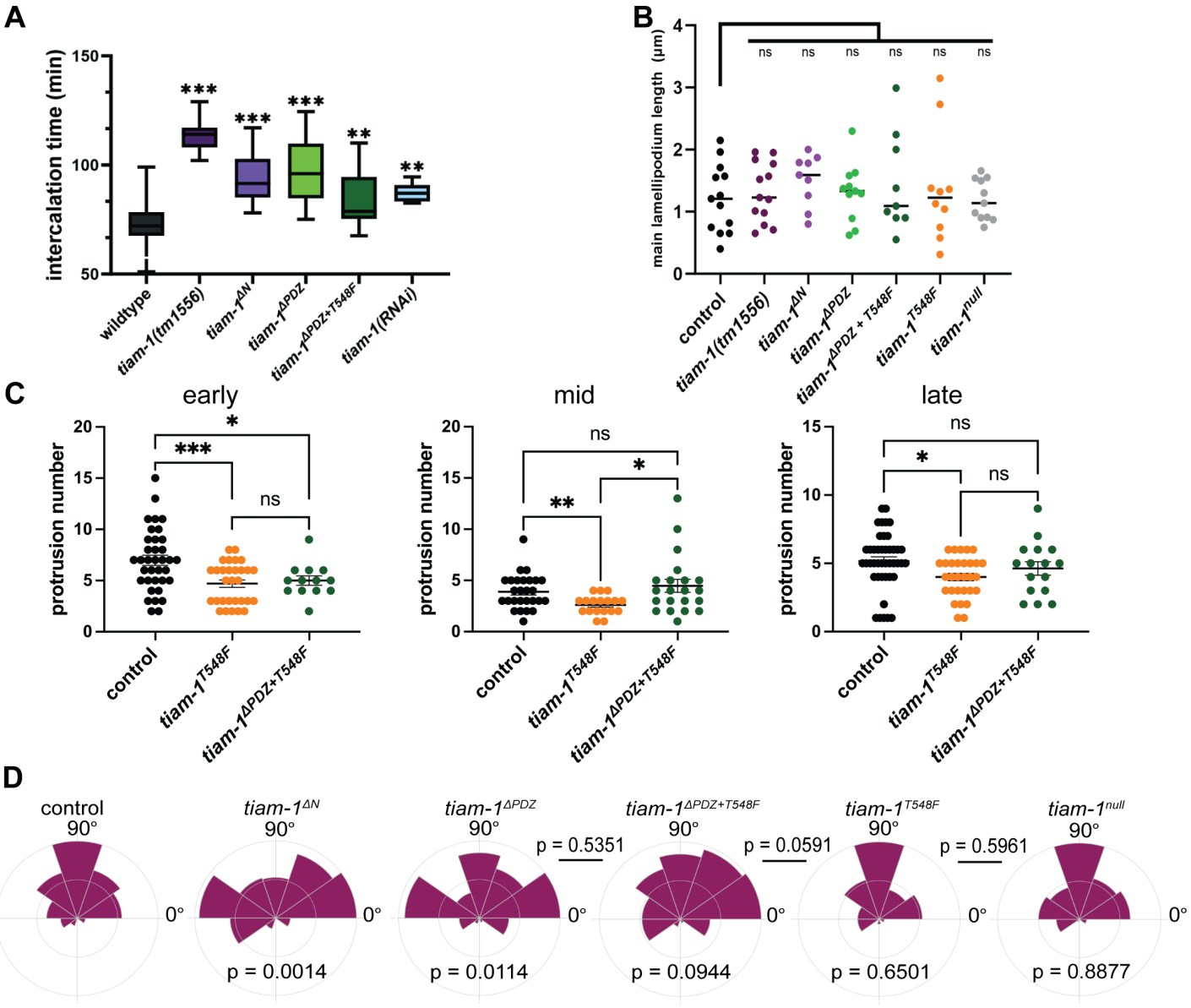

Fig. S3. *tiam-1* N-terminal mutants display defects in dorsal intercalation

(A) Intercalation times of wildtype and *tiam-1* N-terminal deletion mutants. Intercalation times in *tiam-1ΔN*, *tiam-1ΔPDZ* and *tiam-1ΔPDZ+T548F* mutants were significantly different from wildtype. ***, $p < 0.001$; **, $p < 0.01$; unpaired Student's T test.

(B) Base-to-tip length of the main, medial lamellipodium in *tiam-1* mutants at the middle stage of dorsal intercalation. Compared to controls, *tiam-1* mutants show no statistically significant difference in main lamellipodium length. ns, no significant difference; unpaired Student's T test.

(C) Quantification of the number of protrusions generated during early, middle and late stages of dorsal intercalation in control and *tiam-1* mutants. Error bars indicate s.e.m. ***, $p < 0.001$; **, $p < 0.01$; *, $p < 0.05$; ns, no significant difference; one-way ANOVA

(D) Rose plots of the angle of protrusion relative to the cell centroid at the late stage of dorsal intercalation. Annotated p values were calculated using the Mardia-Watson-Wheeler test. p values below the plots compare *tiam-1* mutants with control; p value above the black line compares *tiam-1* mutants.

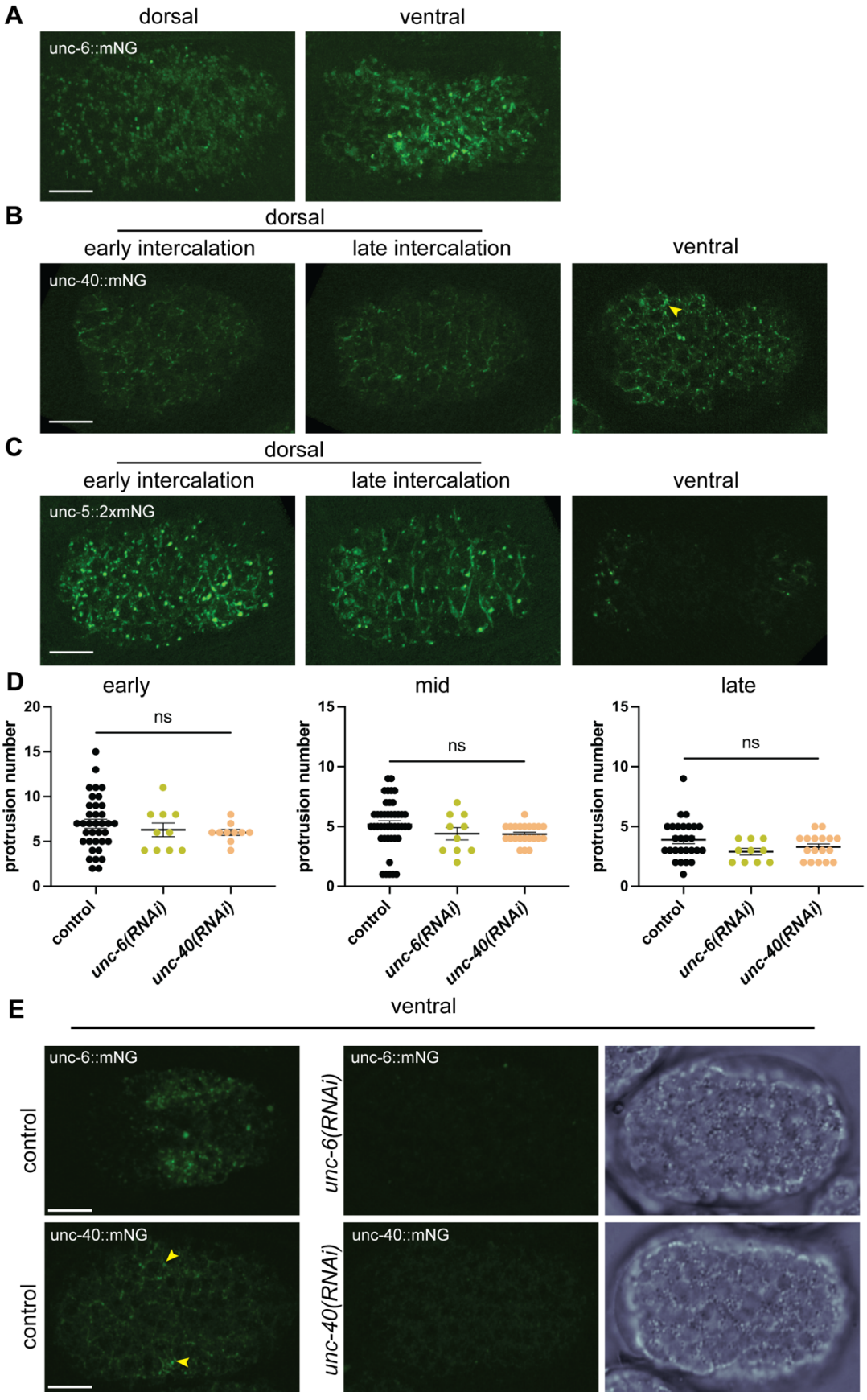

Fig. S4. Netrin pathway components UNC-6 and UNC-40 are not prominently expressed in dorsal epidermal cells and are not involved in regulating protrusion number

(A) Expression of UNC-6::mNG on the dorsal and ventral surfaces of intercalation stage embryos. Scale bar = 10 μm.

(B) Expression of UNC-40::mNG on the dorsal and ventral surfaces of intercalation stage embryos. The arrowhead indicates an example of a bright focus of expression, only visible ventrally. Scale bar = 10 μm.

(C) Expression of UNC-5::2xmNG on the dorsal and ventral surfaces of intercalation stage embryos. Dorsal views are replicated from Fig. 4C. Scale bar = 10 μm.

(D) Quantification of the number of protrusions generated during early, middle and late stages of dorsal intercalation in unc-6 and unc-40 loss-of-function backgrounds. Error bars indicate s.e.m. ns, no significant difference; one-way ANOVA

(E) Diminished expression of UNC-6::mNG and UNC-40::mNG after RNAi knockdown. Images are maximum intensity projections totaling 6 μm in depth, starting just above the surface of the embryo. The corresponding DIC images are single focal planes as a developmental reference. Control images were acquired using the same imaging parameters. Arrowheads indicate examples of bright foci of UNC-40 expression. Scale bar = 10 μm.

Table S1. Strains used in this study

Strain	Genotype
N2	wildtype
EB3014	*tiam-1(dz265)[tiam-1::T to F])I, tiam-1T548F; wdIs52II*
PHX4155	*tiam-1(syb4155)I*
PHX4244	*tiam-1(syb4244)I*
SU1006	*tiam-1(jc86[tiam-1 ΔPDZ+LoxP511])I*
SU1018	*tiam-1(jc86)I; mcEx227[plin-26::vab-10::gfp; pRF4]*
SU1066	*tiam-1(jc105[tiam-1(jc86)*tiam-1 T548F])I*
SU1071	*tiam-1(jc105[tiam-1(jc86)*tiam-1 T548F])I; mcEx227[plin-26::vab 10::GFP; pRF4]*
SU1084	*unc-5(e152)IV; mcEx227[plin-26::vab-10::GFP; pRF4]*
SU951	*tiam-1(dz265)[tiam-1::T to F])I; mcEx227 [plin-26::vab-10::GFP; pRF4]*
SU979	*tiam-1(syb4155)I; mcEx227[plin-26::vab-10::GFP; pRF4]*
SU981	*tiam-1(syb4244)I; mcEx227[plin-26::vab-10::GFP; pRF4]*
CB152	*unc-5(e152)IV*
SU869	*tiam-1(tm1556)I*
SU845	*tiam-1(tm1556)I; mcEx227[plin-26::vab-10::GFP; pRF4]*
NW434	*unc-6(ev400)X*
NK2936	*unc-6(cp190[unc-6::mNG::3xFLAG+LoxP])X*
MT324	*unc-40(n324)I*
NK2672	*unc-40(qy68[unc-40::mNG+LoxP])IV*
NK2673	*unc-5(qy70[unc-5::2xmNG+LoxP])IV*
SU864	*mcEx227[plin-26::vab-10::GFP; pRF4]*
NK772	*unc-119(ed4)III; qyEx115[tiam-1::GFP+unc-119(+)]*
LE137	*unc-73(rh40)I*
SU972	*unc-73(rh40)I 4xoc*
SU973	*tiam-1(tm1556); unc-73(rh40) 4xoc*

Table S2. Oligonucleotides used in CRISPR/Cas9 generation of alleles

Sequence Name	Sequence 5'-3'
Guide 1 for TIAM-1 ΔPDZ	acttgttgttagtactaatg
Guide 2 for TIAM-1 ΔPDZ	aaacttacTCTTGGAGTTAG
TIAM-1 ΔPDZ 5' homology arm Forward	GGCTGCTCTTCgTGGcattgcctcagaaatgaccct
TIAM-1 ΔPDZ 5' homology arm Reverse	GGCTGCTCTTCGCTTTCTGACGAAGTAATCCTCTGCG
TIAM-1 ΔPDZ 3' homology arm Forward	GGCTGCTCTTCgGGTCGAAGAAAGACTCCTTTGACTCCAA GAgta
TIAM-1 ΔPDZ 3' homology arm Reverse	GGGTGCTCTTCgTACcgtttcccaaaatttgggcg
Guide for TIAM-1 T548F	GATGGCTCTGCAAGAATTGTGTTTAAGAGCTATGCTGGAA ACAG
TIAM-1 T548F repair template	GAAAACGGGCTGTGCAAAGTTGGCGATGGCTCTGCAAGA ATTGTTAGTCTTTGAGAAGAAATATGTCAGCGATCTTCGAG AGgtaagggatc